



**HAL**  
open science

## Setting up and modelling of overflowing fed-batch cultures of *Bacillus subtilis* for the production and continuous removal of lipopeptides

Jean-Sebastien Guez, J P Cassar, F Wartelle, P Dhulster, H Suhr

► **To cite this version:**

Jean-Sebastien Guez, J P Cassar, F Wartelle, P Dhulster, H Suhr. Setting up and modelling of overflowing fed-batch cultures of *Bacillus subtilis* for the production and continuous removal of lipopeptides. *Journal of Biotechnology*, 2007, 131, pp.67 - 75. 10.1016/j.jbiotec.2007.05.025 . hal-02938835v1

**HAL Id: hal-02938835**

**<https://hal.science/hal-02938835v1>**

Submitted on 17 Sep 2020 (v1), last revised 19 Jul 2023 (v2)

**HAL** is a multi-disciplinary open access archive for the deposit and dissemination of scientific research documents, whether they are published or not. The documents may come from teaching and research institutions in France or abroad, or from public or private research centers.

L'archive ouverte pluridisciplinaire **HAL**, est destinée au dépôt et à la diffusion de documents scientifiques de niveau recherche, publiés ou non, émanant des établissements d'enseignement et de recherche français ou étrangers, des laboratoires publics ou privés.

**Real Time In Situ Microscopy for Animal Cell-Concentration Monitoring during High Density Culture in Bioreactor**

J.S GUEZ <sup>a\*</sup>, J.Ph CASSAR <sup>a</sup>, F. WARTELLE <sup>c</sup>, P. DHULSTER <sup>d</sup>, H. SUHR <sup>b</sup>

<sup>a</sup> Laboratoire Génie Biologique et d'Automatique - EPU USTL Lille - 59655 Villeneuve d'Ascq Cedex, France

<sup>b</sup> Mannheim University of Applied Sciences, Windeckstr. 110, D-68163 Mannheim Germany

<sup>c</sup> DIAGAST SA, Parc Eura Santé, 251, avenue Eugène Avinée - B.P. 9, 59374 Loos Cedex

<sup>d</sup> Laboratoire de Technologies des Substances Naturelles, EPU USTL Lille - 59655 Villeneuve d'Ascq Cedex, France

(\*) Author for correspondence : [jean-sebastien.guez@polytech-lille.fr](mailto:jean-sebastien.guez@polytech-lille.fr)

Keywords: In Situ Microscopy, Image Analysis, Cellular Concentration, BioProcess Monitoring, Principal Component Analysis

### **Abstract:**

An *in situ* microscope (ISM) device is utilised in this study to monitor hybridoma cells concentration in a stirred bioreactor. It generates images by using pulsed illumination of the liquid broth synchronised with the camera frame generation to avoid blur from the cell's motion. An appropriate image processing isolates the sharp objects from the blurred ones that are far from the focal plane.

As image processing involves several parameters, this paper focuses on the robustness of the results of the cells counting. This stage determines the applicability of the measuring device and has seldom been tackled in the presentations of ISM devices. Calibration is secondly performed for assessing the cell-concentration from the cell automated numeration provided by the ISM. Flow cytometry and hemacytometer chamber were used as reference analytical methods. These measures and the output of the image processing allow estimating a single calibration parameter: the reference volume per image equal to  $1.08 \cdot 10^{-6}$  mL. In these conditions, the correlation coefficient between both reference and ISM data sets becomes equal to 0.99. A saturation of this system during an ultrasonic wave perfusion phase that deeply changes the culture conditions is observed and discussed. Principal component analysis (PCA) is used to undergo the robustness study and the ISM calibration step.

### **Introduction**

The real time measurement of cell-concentration is commonly accepted as a key-point for the development of new monitoring and control strategies in biotechnological processes [Douglas 90]. This is particularly an on-going problem in animal-cell cultures [Konstantinov 94]. Indeed, an on line accurate cellular concentration estimation enables the monitoring of the specific growth rate which is a critical metabolic parameter.

Among all the methods developed for determining the cell-concentration, optical techniques have been increasingly applied [Marose 99] [Ulber 03]. Direct optical technique based on computer imaging were used for offline cell counting and sizing of cell culture sample [Pons 99][Sierachi 98]. The automation of those systems involves circulation loops to take the sample to the microscope focus plane. Automated sampling is not only a complex technique, it is also a risk factor for contamination. In addition, the stress due to the sampling and slide preparation may modify the cells morphology.

In situ microscopes are well suited for in line measurement because they are not invasive and not destructive. They avoid all the microbiological risks relied to sampling. Their design addresses the problem of cell motion due to the broth agitation. Bittner *et al.* proposed a system that mechanically isolates and stops a small volume of broth [Bittner 98]. This system is used within the frame of CHO cell concentration monitoring [Joeris 02].

Suhr *et al.* [Suhr 91][Suhr 95] presented an ISM mounted directly in a port of a bioreactor to generate *in situ* images from the agitated broth using pulse illumination. The sampling volume is now a virtual volume defined by the characteristic of the microscope and the parameters of the associated image processing algorithm. A new version of this ISM has been evaluated on BALB/c mice/mice hybridoma [Guez 2002] and on a yeast strain [Camisard 2000], [Camisard 2002]. The online signal of the cell-concentration provided by the ISM was proved to match with the results of other reference counting methods.

This paper presents results on the estimation of hybridoma cell-concentration during a monoclonal antibody production process. It first gives technical specifications for the *in situ* microscope and details the culture conditions and the analytical methods used to evaluate cell concentration. The second part exhibits the current different stages of the image processing. The third part proposes a PCA to evaluate the robustness of the ISM cell concentration results in relation to the parameters of the image-processing algorithm. Robustness being accessed and the best parameter set being chosen, calibration is performed by using analytical results.

## Material and Method

### The in situ microscope

The in situ microscope [IMV Inline Microvision GmbH, Heidelberg, <http://ism.fh-mannheim.de>] includes a water-immersion objective with a magnification  $\times 40$  and with a numerical aperture 0.75. The microscope tube is enclosed into an 25-mm outer tube with an optical window at the front end. This end is submerged into the broth through the vessel wall in an 25-mm standard port. The port location should correspond to a mixing zone where the broth velocity is optimal so that the sample can be considered as representative of the broth. The location of the port should also take into account bubble of the oxygen supply which can interfere with the images acquired during the process. The submerged end supports an illumination unit with a LED as light source. This entire outer device can sustain the conditions of standard “wet-steam” sterilisation.

Flash illumination with light pulses of about 300 ns in duration avoids blur from cell motion. The pulses are synchronized with a standard CCD camera frame.

The CCD camera (KP- Mi Hitachi 2/3 « CCIR s/x ») has squared  $9\ \mu\text{m} \times 9\ \mu\text{m}$  pixels. Because of the objective magnification  $\times 40$ , each pixel covers an object area of  $0,225\ \mu\text{m} \times 0,225\ \mu\text{m}$ . Hence, an image of a spherical cell that is  $10\ \mu\text{m}$  in diameter consists of about 1540 pixels.

The images are acquired by a standard framegrabber synchronized with the image processing software (WIT, logical vision/Coreco Inc, Canada). Averaging cell numbers over sets of 50 images taken every two hours allows reducing the variability of the calculated cell number per image. Indeed cell number follows a Poisson's law of parameter  $m$  ( $m$  being the expected cell number per image). Standard deviation of the mean number of cells per image is thus kept below  $\sqrt{m/50}$ .

Real-time image processing is then carried out for each image through appropriate algorithms detailed below.

## **Culture Conditions**

The hybridoma cell line tested throughout this study is a BalB/c murine lymphoid cell fused with P3-X63-Ag8.653 murine myeloma. Morphologically, this hybridoma can be considered as an almost perfect spherical object. The robustness of our cell recognition algorithm based on the iterative search of circles in the image will be tested through the recognition of these nearly spherical objects. The average diameter of the studied hybridoma is 13  $\mu\text{m}$  and confirms the values found in literature [Hong 98] [Harada 99]. We notice that in case of heterohybridoma as human/mice, the cells are less regular spherical objects because of the mixed origin of the cellular membrane.

The strain is grown at 37°C in a stirred-tank bioreactor (Discovery 100) with a working volume of 5 litres. Two pitched blades ensure the agitation of the broth. The culture medium is the Dulbecco's Modified Eagle's Media added with 3% heat-inactivated foetal calf serum. Stirring is kept at 40 RPM and pH is controlled at 7.2 by carbon dioxide addition. To prevent contamination and foam formation, overpressure in the vessel is ensured with a surface airflow kept at 10 L/h. Dissolved oxygen is controlled at 25% v/v by injection of pure oxygen. Data acquisition is performed on a personal computer equipped with FIX software. The inoculation rate represents 5 % of the final medium volume and the initial cellular concentration is about  $4 \cdot 10^5$  cell/mL. A 48 hours batch phase is followed by a 288 hours feed phase. The perfusion rate is manually adapted from 0.2 to 0.4  $\text{d}^{-1}$  during the feed phase in order to limit lactic acid and ammonia accumulation in the broth and thus the cell viability decrease. High frequency ultrasonic waves are then used so that the cellular concentration can reach high values within bioreactor. The perfusion rate is set at 0.8  $\text{d}^{-1}$  during this 48 hours phase. The steam-sterilisable resonance chamber (Biosep ADI1015, ApplisSens) is mounted on the top of the reactor on a standard 12-mm port (Figure 1). An acoustic resonance field causes an active cell aggregation in the separation chamber of the resonator. Two peristaltic pumps are required for harvesting the clarified culture and recirculating the cell suspension. Aggregates of cells sediment to the bioreactor and are suspended again by stirring. To maintain stable thermal

conditions in the separation chamber, cooling is ensured with insufflating air at 10-L/min. This system was already applied successfully on hybridoma cells [Trampler 94] [Phylis 95] [Bierau 98].

### **Cell concentration.**

Two different methods of assessing cell concentration are used. First, a routine procedure is carried out using the Trypan blue exclusion principle. 100  $\mu$ L of the sample is diluted with 100  $\mu$ L of Trypan blue and cells are numerated on a Malassez counting chamber after a 5 minutes incubation period at 20°C. Second, a fluorescence-based method is used. (Live/Dead® Viability/Cytotoxicity assay kit, Molecular Probes). The kit provides a two-color fluorescence assay based on the simultaneous determination of live and dead cells so that the total number of cells can be measured. Two probes, calcein AM and ethidium homodimer are used to estimate respectively: intracellular esterase activity and plasma membrane integrity [Hayes 1994]. Prior to the assay, samples are washed by centrifugation at 700 g for 15 minutes. Washing is performed with sterile tissue culture-grade D-PBS (KCl (0.2 g/L), KH<sub>2</sub> PO<sub>4</sub> (0.2 g/L), NaCl (8 g/L) and Na<sub>2</sub>HPO<sub>4</sub> (1,15 g/L)) to remove serum because serum esterases can cause some increase in extracellular fluorescence by hydrolyzing calcein AM. Cell staining is carried out with optimised dye concentration determined with a conventional fluorescence microscope (Optiphot, Nikon). We determined an optimal concentration of 0.1  $\mu$ M for calcein AM and 8  $\mu$ M for ethidium homodimer. A recommended range of 1,0.10<sup>6</sup> to 1,5 10<sup>6</sup> single-cells is incubated in 1 mL D-PBS and 100  $\mu$ L of each reagents for 10 minutes at room temperature. Samples are injected in a Facscalibur flow cytometer (Becton Dickinson) working at a high flow rate (60  $\mu$ L/min). Cell Quest software performs data processing and classical quadrant statistics. A defined number of events are counted upon time in order to calculate the cellular concentration.

### **Image Processing**

The frame-grabber delivers 8 bits grey valued 659x494 frames (Figure 2). Most of the objects contained in images are far from the focus plane. Cells located between the illumination diode and

the focus plane can act as lenses leading to bright spots with smooth edges while the other ones are dark and blurred. Grey scaled image pre-processing into binary image must distinguish these objects from the sharp ones that belong to the focal plane. It is usually based on the setting of an appropriate threshold in the grey levels of the image. Automatic calculation of such a threshold that bears on the existence of at least two peaks in the histogram of the grey levels [Sierachi 98][Vicente 96] can not be used as the grey-level histogram in ISM-Images shows only one dominant peak. Indeed, grey levels do not contain pertinent information in our specific case. Therefore, an edge enhancement is applied to the original image through a spatial highpass filter before thresholding. Threshold is set in a very flat zone of the resulting histogram and thus robustness of the result is ensured.

The cell recognition stage is provided with a binary image. The cell membranes are matched with circles of specific sizes. Our cell recognition algorithm uses the circular-Hough transformation for an iterative search of circles in the image. The circular-Hough transform provides, for each point considered as a circle center, a value indicating which proportion of the perimeter of a given radius circle coincides with white image-pixels. Thresholding this information allows locating the candidates for cell recognition. The level of the threshold indicates the level of completeness that must be achieved before a cell is selected. The iterative search runs from large to small diameters objects.

A cell selected for a given radius contributes to the count rate of the size class corresponding to this radius. Then the search is performed again for the next radius. Figure 3 shows the result of the recognition process on the image presented in Figure 2. The size range of the search is set from 10 to 34 pixels corresponding to particles from 4.5 to 15.3  $\mu\text{m}$  of diameter.



## Robustness study

The study aim is exhibiting the influence of the set of parameters involved in the image-processing algorithm on the cell concentration results. Indeed, it has to be proved before calibrating the ISM that these parameters only modify the scale of the concentration curves but not their shape.

The result, for a given parameter set  $j$ , is a curve that gives at each time  $t_i$  the mean number of cells in an image, called  $y_j(t_i)$ . If the parameters do not influence the shape of the  $y_j(t_i)$  - curves each curve can be deduced from a single time function  $f(t_i)$  by using a factor “ $a_j$ ”:  $y_j(t_i) = a_j f(t_i)$ . In this case, the different values of the  $a_j$  coefficients directly express how the parameters value change the reference volume for the cell counting. However, if the parameters do influence the shape of the time functions, each time function can be expressed as a specific linear combination of a set of  $K$  reference time functions  $f_k(t_i)$ . Gathering the  $y_j(t_i)$  values in a single vector  $\mathbf{y}(t_i)$  allows writing:

$$\mathbf{y}(t_i) = \sum_{k=1}^K f_k(t_i) \mathbf{a}_k \quad (1)$$

The normalised vectors  $\mathbf{a}_k$  are linearly independent.  $K$  is the dimension of the space of vectors  $\mathbf{y}(t_i)$  – i.e. the number of functions  $f_k(t_i)$  that are needed to reconstruct all curves  $y_j(t_i)$ . The non-influence of parameters with respect to the curve shapes is equivalent to  $K = 1$ .

Principal component analysis (ref) provides a very powerful tool to answer the problem of finding the dimension  $K$  and of estimating the corresponding  $f_k$  - functions.

Let the information be gathered in a single matrix  $\mathbf{Y} = [\mathbf{y}(t_1) \ \mathbf{y}(t_2) \ \cdots \ \mathbf{y}(t_n)]'$ . From (1) and the properties of the vectors  $\mathbf{a}_k$  it can be deduced that:

$$\mathbf{Y} \mathbf{a}_k = [f_k(t_1) \ f_k(t_2) \ \cdots \ f_k(t_n)]' = \mathbf{f}_k \quad (2)$$

This expression is the estimate of the time function whose values are the entries of the vector  $\mathbf{f}_k$ .

PCA methods [Ramsay 97] provide the most significant functions from eigenvectors of the  $\mathbf{Y}'\mathbf{Y}$  - matrix

The K-dimension is obtained from the number of eigenvalues that are considered as different from zero. The  $f_k$  -vectors associated with these greatest eigenvalues are called principal components

Let the **F**-matrix gather the principal components and the **A**-Matrix the corresponding eigenvectors.

A filtered estimation  $\hat{Y}$  can be substituted to **Y** and is computed from the principal components  $F=YA$ .

$$\hat{Y} = FA' = Y A A' \quad (3)$$

The columns of the **A'**-matrix thus indicate how the principal components have to be combined in order to retrieve a filtered version of the original curves. Analysing of how this combination is performed for every curve allows coming at a conclusion about the similarity of their shapes.

### **ISM calibration**

This part aims at finding the conversion coefficient that allows estimating the cell concentration from the number of cells per image provided by the ISM. The difficulty is that the detected objects belong to a virtual probe volume. The optical device and the CCD sensor size define the lateral borders of the probe volume, while its depth depends on the parameters of the pre-treatment process. This means that the algorithm discards the objects from outside of the sharpness depth.

This can be expressed as  $c(t) = a y(t)$  where  $c(t)$  is the cell concentration (cell/ml) and  $y(t)$  the ISM measurement (cell/image). The coefficient “a” can be interpreted as the inverse of the reference volume expressed in ml/image and is the ISM calibration parameter.

Finding the conversion coefficient needs alternate measurements on cell concentrations to be performed. Cell concentration analyses are carried out during the cell culture. They provide at each time a vector that gives the references of the cell concentration. These vectors are gathered in the matrix  $X = [x(t_1) \quad K \quad x(t_j) \quad K \quad x(t_m)]$ .

The calibration procedure aims at finding the global calibration factor “a” that takes into account the both analysis results. Therefore, the calibration procedure is divided into three main stages:

- data processing in order to handle missing analysis data and to estimate the ISM responses at times  $t_j$  because the times  $t_i$  and  $t_j$  do not correspond exactly;
- estimation of the first principal components from PCA to reduce influence of discrepancies between the analytical results;
- computation of the regression factor with respect to the correlation between ISM results and filtered analysis.

The first stage is achieved by linear interpolation procedures. In the second stage  $\mathbf{X}$  is filtered from PCA (by keeping a reduced number of principal components) to give the better estimate of the cell concentration from analytical results. In the third stage, factor 'a' of the regression model is obtained from the least square estimation procedure between the filtered X-values and the mean cell numbers calculated with parameter k.

## Results and Discussion

The algorithm used for the cell counting involves three parameters. The first one is the size of the high pass filter that enforces the shape detection. The second one is the value of the threshold used after the Hough transformation to decide the matching with a circle. The third one is the number of circles examined, beginning from 15,3  $\mu\text{m}$  diameter circles and decreasing iteratively 0.9  $\mu\text{m}$  by 0.9  $\mu\text{m}$  until the last circle diameter is reached.

Table 1 gives the values of these parameters and the corresponding number of parameter sets.

Figure 4 presents the curves of the mean cell numbers that are obtained with the chosen parameter sets.

Figure 5 shows the projections of the  $y_j(t_i)$  curves in the first principal plane. The co-ordinates in this plane are the columns of the matrix  $\mathbf{A}'$  restricted to dimension 2. For each point labelled by a number j, they give the combination of the two first principal components that are needed to recompose a filtered version of the original curve  $y_j(t_i)$  associated with the parameter set j. A projection close to the unit circle indicates that two principal components are sufficient to well

regain the curve and thus the dimension  $K$  is equal to 2. It can be noticed that the projections of the parameters sets from 1 to 5 corresponding to  $5 \times 5$  filter size are farther from the unit circle indicating the need of a third principal component. This is why these parameter sets are excluded for the rest of the study. The other parameter sets projections are close to the unit circle.

The closer the projections are, the more similar the original shapes are. Taking this into account, we can analyse the group of parameter sets exhibited in figure 5 as follows: the filter size has almost no influence on the shape of the curve. The parameter sets that are only distinguished by the value of this parameter (by example 6-15, 7-16) belong to the same group. The two groups 11-20-12-21 and 8-17-10-19 correspond to a strategy that compensates a more demanding threshold by an increase of the number of circles used in the Hough transformation. However, all these influences are weak and can be considered as negligible. At this stage, we can conclude about the influence of the parameter sets that:

- The filter size exerts no influence if its value is limited between 10 and 20.
- Threshold and number of circles have a weak influence in the ranges that have been explored and lead to variations in the curves shape that are insignificant regarding the dispersion of the acquired data.

Now let us consider the calibration stage. Figure 6 gives the cell concentration obtained from both kinds of analysis. As we have only two kind of analysis only one principal component as to be kept and then it is the mean value of the curves. In figure 5, this principal component is projected (bold circle) onto the same principal plane than the ISM data. It can be deduced that the shape corresponding to the reference analyses is very close to the shape corresponding to the curves given by parameter sets 9 -18 and 10-17. For the parameter set 9 ( $k=9$ ) chosen among these points, figure 7 exhibits the regression expressed in between analysis data estimated as the first principal component and corresponding ISM data. It shows that the last data point at maximum concentration is far from the linear regression model. Hence, the linear model may not be the best calibration model if the maximum concentration is included. Excluding this last analysis, the projection onto

the first principal plane of ISM results becomes closer to the parameter sets 7 and 16 (diamond in Figure 5).

With this restricted set of analyses, results of the regression with the parameter sets corresponding to a filter size of 10x10 leads to the results shown in Table 2 (it could have been indifferently a filter size of 20x20 as it was showed previously). The term “Slope” indicates the regression coefficient ‘a’, from which the reference volume is inferred. The obtained standard deviations do not differ significantly, so that the robustness of the algorithm according to changes in the set of parameters is confirmed. However, it can be seen that the reference volume increases if the threshold decreases. This behaviour is to be expected because lower thresholds allow the detection of less sharp cell images.

The regression model calculated for parameter set  $k=7$  gives a value for ‘a’ equal to 0.99. Concentrations values calculated using this model and the corresponding ISM data are given figure 8. An interval of confidence, associated with a 5% risk, is computed for each estimate from the error variance estimation. The comparison with the original analysis values shows the quality of the calibration for concentration below  $4.5 \cdot 10^6$  cells/ml.

Let us now focus on the observed saturation. The deviation of the last analysis point is clearly related to the perfusion phase. The resonance field both causes an increase in the cell concentration and an active cell aggregation phenomenon that is displayed in Figure 9. As the image-processing algorithm is not well suited to undergo the counting of the cells belonging to flocs of cells, the cellular concentration may thus be under-estimated. Moreover, the evolution of the optical characteristics of the broth was noticed: images become darker and the cells got more blurred than at the beginning of the process. That may also contribute to the underestimation of the number of cells.

## **Conclusion**

A very careful procedure has been proposed to establish how the image-processing algorithm is robust and efficient when faced with spherical or nearly spherical objects. For concentrations below  $4.5 \cdot 10^6$  cells/ml, the ISM gives a good on-line estimate of the cell-concentration and is robust faced to image processing parameter changes. Indeed, the selected set of parameters allows the ISM cell-concentration curve to fit almost perfectly the reference method results and the correlation coefficient between both reference and ISM data sets is then equal to 0.99. The calibration method applied for this set of parameters corresponds to a  $1.08 \cdot 10^{-6}$  mL reference volume that can be considered as a reference volume for further ISM utilisation. Thus, the presented system could be used in an extensive way for enhancing process control in the frame of agitated broth cell cultivation.

## **Acknowledgements**

This work was supported by:

DIAGAST SA, Parc Eura Santé, 251, avenue Eugène Avinée - B.P. 9, 59374 Loos Cedex

Pr. Joël Mazurier for flow cytometry analysis, UMR N°8576 CNRS/USTL Lille

## References

- Bierau, H., Perani, A., Al-Rubeai, M. and Emery, A.N. (1998) A comparison of intensive cell culture bioreactors operating with hybridomas modified for inhibited apoptotic response. *J. Biotechnol.* 62, pp.195-207.
- Bittner, C., Wehnert, G. and Scheper, T (1998) In situ microscopy for on-line determination of biomass. *Biotechnol. BioEng.* 60, 1, pp. 24-35.
- Camisard, V., Brienne, J.P., Baussart, H., Cassar, J.P. (2000) Effects of osmotic pressure shocks on yeast morphology: Experimental study and modelling. First International Conference on Simulation in Food and Bio industries, Nantes, France.
- Camisard, V., Brienne, J.P., Baussart, H., Hammann, J. and Suhr, H. (2002) Inline Characterization of Cell Concentration and Cell Volume in Agitated Bioreactors Using in Situ Microscopy: Application to Volume Variation Induced by Osmotic Stress. *Biotechnol. BioEng.*, 78, pp. 73-80.
- Guez, J.S., Cassar, J.Ph. (2002) In Situ Microscopy for In-line Monitoring of Hybridomal Cell Culture in Agitated Bioreactor. National Conference on Signal and Image Processing in Food and Biotechnological Processes, Nantes, France. pp. 110-115.
- Hayes, A.W. (1994) Principles and Methods of Toxicology. Raven Press, Third Edition, pp. 1231-1258.
- Harada, M., Masashi, S., Kitamori, T. and Sawada, T. (1999) Sub-Attomole Molecule Detection in a Single Biological Cell in-vitro by Thermal Lens Microscopy. *Anal. Sci.* 15, pp. 647-650.
- Hong, M.K., Jeung, A.G., Dokholyan, N.V., Smith, T.I., Schwettman, H.A., Huie, P. and Erramilli, S. (1998) Imaging single living cells with a scanning near-field infrared microscope based on a free electron laser. *Nucl. Instrum. Meth. B*, 144, pp. 246-255.
- Joeris, K., Frerichs, J-G., Konstantinov, K. and Scheper, T. (2002) *In-situ* microscopy: Online process monitoring of mammalian cell cultures. *Cytotechnology.* 38, pp. 129-134.

- Kell, D.B., Markx, G.H., Davey, C.L. and Todd, R.W. (1990) Real time monitoring of cellular biomass: Methods and Applications. *Trends Ana. Chem.* 9, 6, pp. 190-194.
- Konstantinov, K., Chuppa, S., Sajan, E., Tsai, Y., Yoon, S. and Golini, F. (1994) Real-time Biomass-concentration Monitoring in Animal-cell Cultures. *Tibtech.* 12, pp 324-333.
- Kosebalaban, F. and Cinar, A. (2001) Integration of Multivariate SPM and FDD by Parity Space Technique for a Food Pasteurization, *Comput. Chem. Eng.* 25, pp. 423-491.
- Kourti, T. and MacGregor, J.F., (1995) Process analysis, monitoring and diagnosis, using multivariate projection methods. *Chemometr. Intell. Lab.* 28, 1, pp. 3-21.
- Phylis, W.S., Trampler, F., Sonderhoff, S., Groeschl, M., Kilburn, D.G. and Piret, J.M. (1995) Batch and semi-continuous aggregation of hybridoma cells by acoustic resonance fields. *Biotechnol. Progr.* 11, pp. 146-152.
- Pons, M. N., Vivier, H. (1999) Biomass Quantification by Image Analysis. *Adv. Biochem. Eng.* 66, pp. 135-174.
- Ramsay, J. O., Silverman, B. W. (1997) *Functional Data Analysis* Springer. ISBN 0-387-94956-9
- Suhr, H., Speil, P., Wehnert, G. and Storhas, H. (1991) Bioreaktor mit In Situ Mikroskopsonde und Messverfahren. *Deutsche Offenlegungsschrift* 4032002.
- Vicente, A., Meinder, J. M., Teixeira, J. A. (1996) Sizing and Counting of *Saccharomyces cerevisiae* Floc Population by Image Analysis, Using an automatically Calculated Threshold. *Biotechnol. BioEng.* 51, pp 673-678.
- Sierachi, M. E., Viles, C.L. (1990) Enumerating and Sizing of Micro-organism using Digital Image Analysis. In: Wilkinson, M.H.F. and Schut, F. (Eds.) *Digital Image Analysis of Microbes. Modern Microbiological Methods.* Wiley.



Sühr, H., Wehnert, G., Schneider, K., Bittner, C., Scholz, T., Geissler, P., Jähne, B. and Scheper, T. (1995) *In situ* microscopy for on-line characterization of cell populations in bioreactors, including cell-concentration measurement by depth from focus. *Biotechnol. Bioeng.* 47, pp. 106-116.

Trampl, F., Sonderhoff, S.A., Pui, P.W.S., Kilburn, D.G. and Piret, J.M. (1994) Acoustic cell filter for high density perfusion culture of hybridoma cells. *Bio/Technology*, 12, 3, pp. 281-284.

Ulber, R., Frerichs, J-G. and Beutel, S. (2003) Optical sensor systems for bioprocess monitoring. *Anal. Bioanal. Chem.* 376, pp. 342-348.

Figure 1: Diagram of the In Situ Microscope mounted in a bioreactor growing cells suspended in a nutrient medium. Pump 1 and 2 are respectively the feed and harvest pumps. Pump 3 is the clarified culture medium harvest pump. Pump 4 is the recirculation pump.

Figure 2: Original ISM image of the stirred culture broth. Hybridomal cells occur as individual cells or as twins in the case of mitosis. Cells belonging to the virtual probe volume appear with sharper edges.

Figure 3: Objects recognised as cells after the pre-processing phase and the cell recognition phase.

Figure 4: Mean cell number curves (cells/image) during the time of the culture. Each curve corresponds to a set of parameters (see Table 1).

Figure 5: Coordinates in the first principal plane of cell-number per images curves. Projections are numbered according to parameter sets in Table 1.  $\circ$  and  $\diamond$  are the projection of the first principal component of the analytical results respectively for 20 and 19 values.

Figure 6: Evolution of the hybridoma concentration results (cell/ml) during the culture (h).

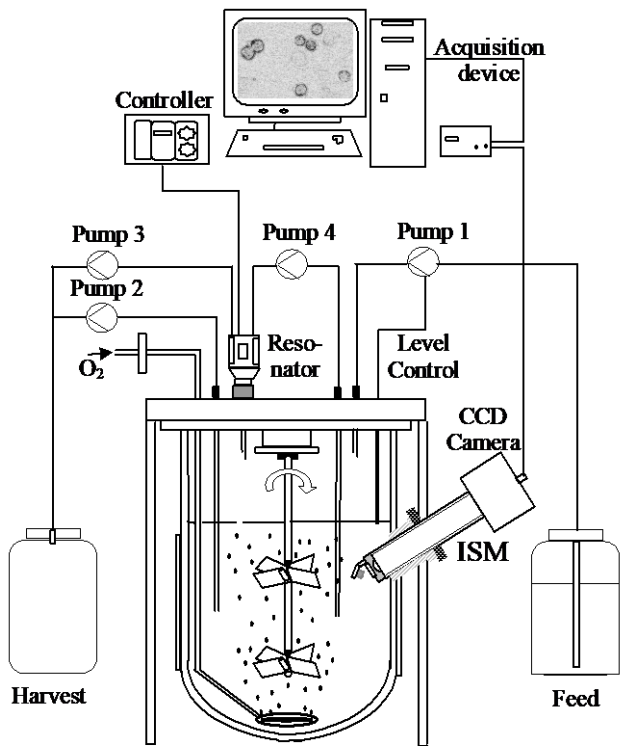
Figure 7: Regression model between ISM cell-concentration results (cells/image) based on parameter set 9 and reference data from hemocytometry (\*) and from flow cytometry (o).

Figure 8: Final ISM cell-concentration results (—) and the 5% confidence interval (---) considering parameter set 7 and only keeping first 19 analysis to avoid the saturation. Results are compared with hemocytometry (\*) and flow cytometry (o).

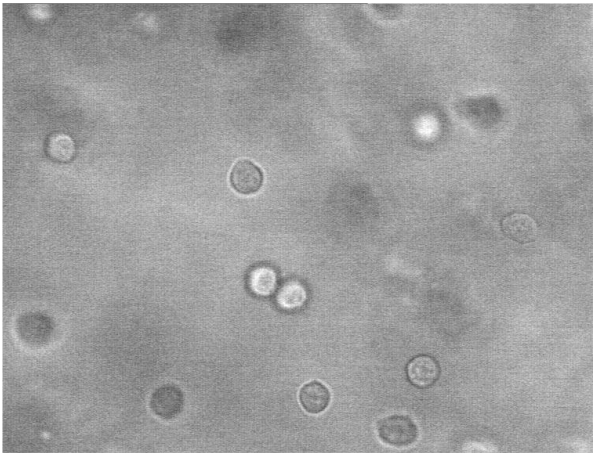
Figure 9: 8 bit gray scaled image of cell aggregates due to the acoustic resonance field during the ultrasonic perfusion phase.

Table 1: Parameter sets used to specify filter-size, binarisation-threshold and number of circles in the image processing algorithm.

Table 2: Regression results for filter size 10x10. The data-point at maximum concentration is excluded from this analysis in order to avoid saturation.



**Figure 1:**



**Figure 2:**

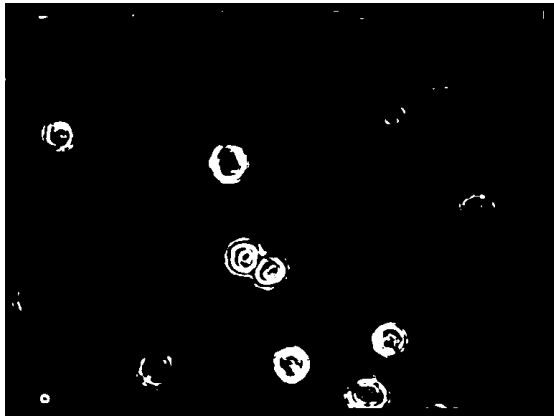


**Figure 3:**

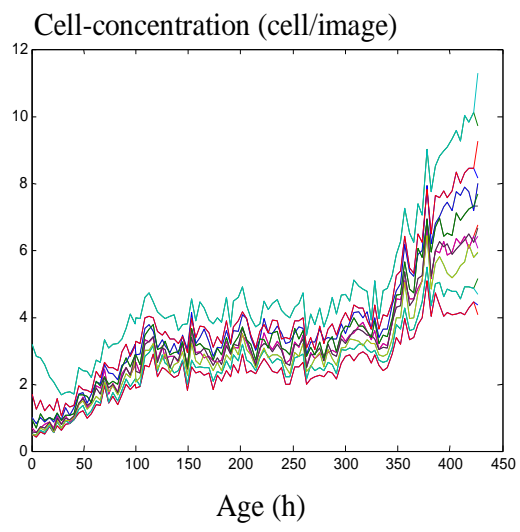


**Figure 4:**



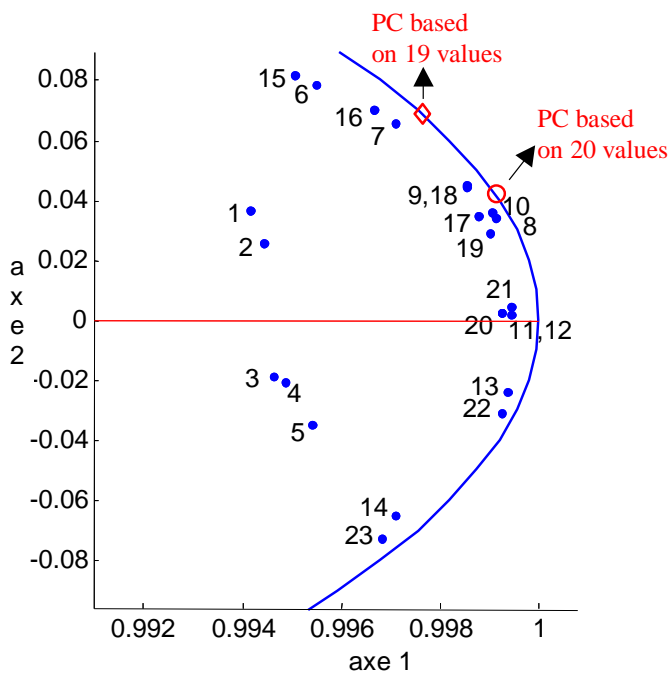


**Figure 5:**

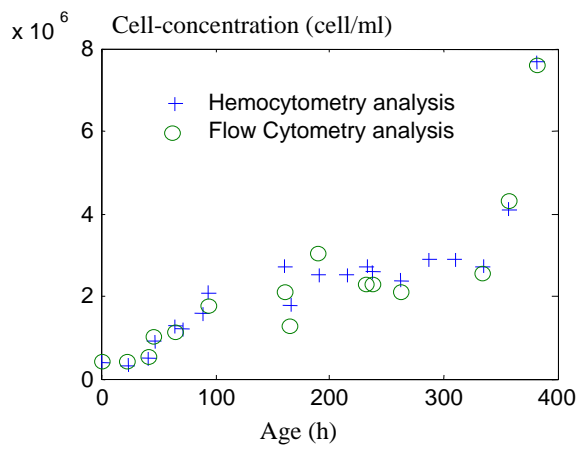


**Figure 6:**

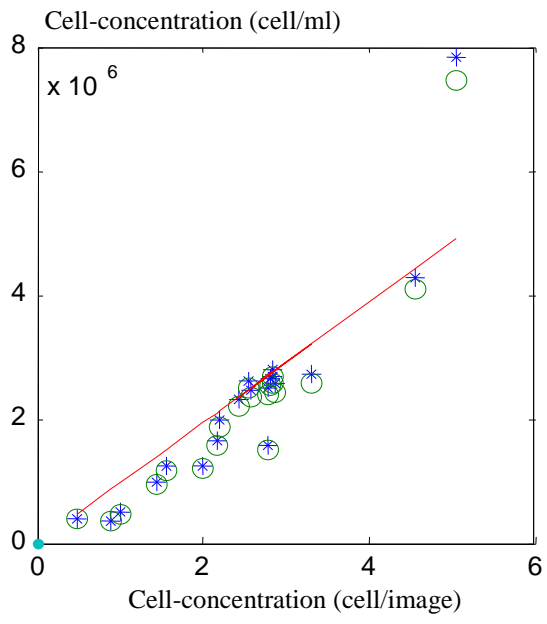


**Figure 7:**

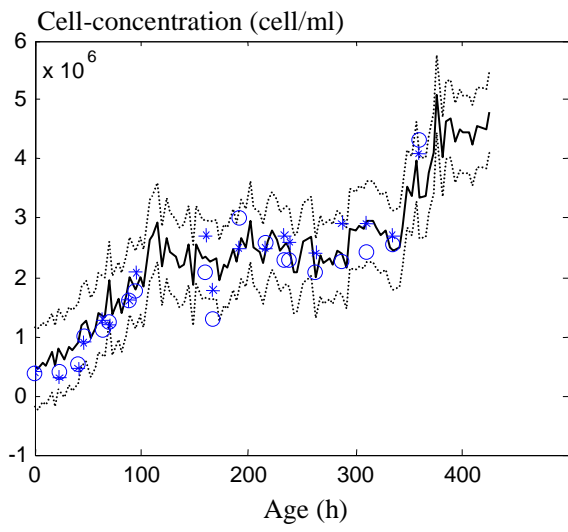


**Figure 8:**

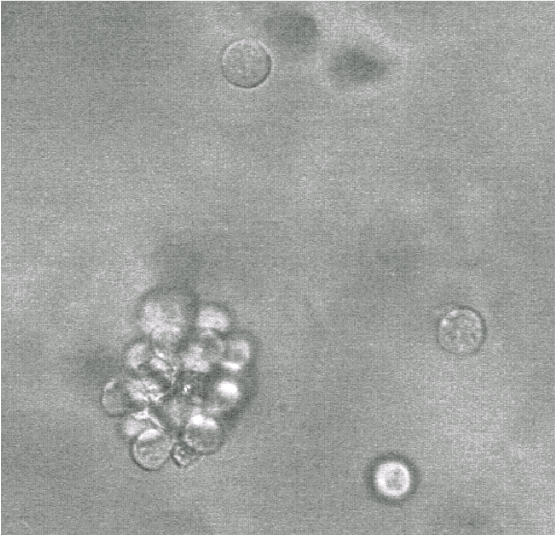


**Figure 9:**

**Table 1**

		Filter size								
		5x5			10x10			20x20		
Number of circles	Threshold	10	11	12	10	11	12	10	11	12
		200	1	2	3	6	7	8	15	16
180	4	5	/	9	10	11	18	19	20	
160	/	/	/	12	13	14	21	22	23	

**Table 2**

<b>Parameter set</b>	<b>6</b>	<b>7</b>	<b>8</b>	<b>9</b>
Slope				
' $10^5$ image/ml	1.00	9.26	7.88	8.55
Standard deviation				
' $10^5$ image/ml	3.37	3.35	3.18	3.23
Reference volume				
' $10^{-6}$ ml/image	9.96	1.08	1.27	1.17
<b>Parameter set</b>	<b>11</b>	<b>12</b>	<b>13</b>	<b>14</b>
Slope				
' $10^5$ image/ml	6.80	7.34	6.40	5.30
Standard deviation				
' $10^5$ image/ml	3.35	3.32	4.09	4.97
Reference volume				
' $10^{-6}$ ml/image	1.47	1.36	1.56	1.89